



A wearable sensor for the detection of sodium and potassium in human sweat during exercise

Paolo Pirovano^a, Matthew Dorrian^a, Akshay Shinde^a, Andrew Donohoe^a, Aidan J. Brady^b, Niall M. Moyna^b, Gordon Wallace^c, Dermot Diamond^a, Margaret McCaul^{a,*}

^a Insight Centre for Data Analytics, National Centre for Sensor Research, Dublin City University, Glasnevin, Dublin 9, Ireland

^b School of Health and Human Performance, Dublin City University, Dublin 9, Ireland

^c ARC Centre of Excellence for Electromaterials Science, University of Wollongong, Wollongong, NSW, 2522, Australia

ARTICLE INFO

Keywords:

Wearable sensors
Sweat
Electrolyte monitoring
Real-time sensing
Ion-selective electrodes
Sodium
Potassium

ABSTRACT

The SwEatch platform, a wearable sensor for sampling and measuring the concentration of electrolytes in human sweat in real time, has been improved in order to allow the sensing of two analytes. The solid contact ion-sensitive electrodes (ISEs) for the detection of Na^+ and K^+ have been developed in two alternative formulations, containing either poly(3,4-ethylenedioxythiophene) (PEDOT) or poly(3-octylthiophene-2,5-diyl) (POT) as a conductive polymer transducing component. The solution-processable POT formulation simplifies the fabrication process, and sensor to sensor reproducibility has been improved via partial automation using an Opentron[®] automated pipetting robot. The resulting electrodes showed good sensitivity (52.4 ± 6.3 mV/decade (PEDOT) and 56.4 ± 2.2 mV/decade (POT) for Na^+ ISEs, and 45.7 ± 7.4 mV/decade (PEDOT) and 54.3 ± 1.5 mV/decade (POT) for K^+) and excellent selectivity towards potential interferents present in human sweat (H^+ , Na^+ , K^+ , Mg^{2+} , Ca^{2+}). The 3D printed SwEatch platform has been redesigned to incorporate a double, mirrored fluidic unit which is capable of drawing sweat from the skin through passive capillary action and bring it in contact with two independent electrodes. The potentiometric signal generated by the electrodes is measured by an integrated electronics board, digitised and transmitted via Bluetooth to a laptop. The results obtained from on-body trials on athletes during cycling show a relatively small increase in sodium (1.89 mM–2.97 mM) and potassium (3.31 mM–7.25 mM) concentrations during the exercise period of up to 90 min.

1. Introduction

Research into wearable sensors has experienced significant growth in recent years, enabled by advances in electronics, materials and analytical science [1–3]. However, the vast majority of devices currently on the market are based on physical sensors, such as temperature, pressure, movement and heart-rate monitors, as incorporation of biochemical sensors into wearable platforms poses complex challenges [4]. Accessing biological fluids such as blood and interstitial fluid also represents a significant obstacle, as the skin barrier must be breached in some manner to access the sample, leading to issues of wearer comfort and potential infection. In contrast, sweat represents a readily accessible biological fluid, whose composition includes electrolytes and metabolites which can provide information on the health status and physical condition of the individual [5]. Electrolytes such as sodium and potassium ions are related to hydration status, and can be used to diagnose and track the efficacy of treatments for conditions such as

cystic fibrosis [6], and electrolyte imbalances [7]. Real-time tracking of electrolyte concentrations in sweat can therefore provide important information for biomedical diagnostics, assessing therapeutic interventions and sports performance optimisation. Electrochemical (potentiometric or galvanometric) sensors constitute one of the main approaches to wearable biochemical sensors. Obtaining the lifetime and stability for tracking key biochemical targets during normal daily activity is more challenging for biochemical sensors compared to the much better-behaved physical transducers. Current research on potentiometric, and other electrochemical sensors has been recently reviewed but new systems are reported regularly. Rogers and collaborators demonstrated a system capable of monitoring pH, lactate, glucose, and chloride; using a battery-free device. Javey and Crespo have reported patch sensors for the measurement of H^+ , Na^+ , K^+ and Cl^- [8–10], while Bertsch focused on NH_4^+ [11], and Andrade on total ionic content [12]. Gerasopoulos developed a lactate-sensing patch based on an organic electrochemical transistor and

* Corresponding author.

E-mail address: margaret.mcaul@dcu.ie (M. McCaul).

<https://doi.org/10.1016/j.talanta.2020.121145>

Received 1 April 2020; Received in revised form 2 May 2020; Accepted 8 May 2020

Available online 30 May 2020

0039-9140/ © 2020 The Author(s). Published by Elsevier B.V. This is an open access article under the CC BY license (<http://creativecommons.org/licenses/by/4.0/>).

chronoamperometric sensors have also been reported for ethanol [13], urea [14] and caffeine [15]. We have previously reported a watch-type platform for sweat electrolyte monitoring called 'SwEatch' [16,17] and an analogous patch system [18], both of which are capable of drawing sweat from the skin of the wearer through thread fluidics, and tracking the concentration of Na^+ ions in exercise generated sweat through embedded potentiometric sensors. In this article, we report further advances which improve the design of the SwEatch platform and extend its use to the analysis of multiple electrolytes. The modular design of the platform easily allows the selection of the analyte by simply replacing the electrode component. The device was characterised via lab testing prior to use in trials with volunteer athletes for a period up to 90 min in the School of Health and Human Performance at Dublin City University.

2. Materials and methods

2.1. Materials

Sodium chloride, tetrahydrofuran (THF), 3,4-ethylenedioxythiophene (97%, EDOT), 4-tert-butyl-calix [4]arene-tetraacetic acid tetraethyl ester (sodium Ionophore X), valinomycin (potassium ionophore I), tridodecylmethylammonium chloride (TDMACl), potassium tetrakis(4-chlorophenyl)-borate (KTCBP), high molecular weight poly(vinyl chloride) (PVC), bis(2-ethylhexyl) sebacate (DOS), poly(methyl methacrylate-co-butyl methacrylate) (PMMA-co-BMA), bis(2-ethylhexyl) phthalate (DEHP), poly(3-octylthiophene-2,5-diyl) (POT) were all purchased from Sigma-Aldrich, Ireland and were of selectophore grade where available. 1-Hexyl-3-methylimidazolium tris(pentafluoroethyl)trifluorophosphate (HMIM FAP) was purchased from Merck. 1-Ethyl-3-methylimidazolium bis(trifluoromethane)sulfonimide (EMIM NTf₂, 99.5%) was purchased from Iolitec, Germany. All chemicals were employed without further purification. Carbon ink (C2030519P4) and dielectric ink (D50706D4) were purchased from Gwent Group, UK and used without modification. Deionised water obtained from a Milli-Q reagent grade purification system was used for the preparation of all aqueous solutions. PET sheets were purchased from MacDermid, UK, and 500 μm PMMA sheets from Peerless Plastics & Coatings Ltd, UK. The device battery (3.7 V, 155 mAh) and electronics board were provided by Shimmer Ireland, DCU Alpha, Glasnevin, Dublin, Ireland. Platforms parts including the enclosure and reservoir fabricated using an Object260 Connex1 Polyjet 3D Printer (Stratasys, Rheinmünster 77836 Germany). The build materials were VEROBLA-CKPLUS RGD875, a rigid acrylic based proprietary resin, and TANG-OBLACK PLUS FLX980, a rubber-like acrylic resin, from Stratasys, UK. The support material was OBJET Support SUP706. Flexible polymer provides a sealing and press fit between casing and dual Macroduct. Casing assembly consist two-part design, put together with counter sink M3X12mm nylon nut and bolt arrangement. For the fluidics transport cotton threads extracted from medical gauze (length 7 cm) were used. The reservoir uses cellulosic absorbent material "Superior Cleanroom Products Three Layer Compo Wipe", Part No 87112, 8 layers, are cut by laser in the appropriate shape.

2.2. Instrumentation

A DEK 248 semi-automatic screen printer was used for the deposition of conductive and dielectric layers in the electrodes. PMMA parts were cut with an Epilog Zing Laser Cutter. Electrodeposition of PEDOT was carried out using a CH Instruments CHI630B electrochemical analyser. Potentiometric measurements were recorded using a multi-channel Lawson Labs MCV potentiometer, with a double junction Ag^+/AgCl electrode (Sigma-Aldrich, Ireland); cell potentials for the integrated electrodes were measured using the Shimmer PCB and acquired with Consensys v1.5.10 software (Shimmer Ltd.).

2.3. Electrode fabrication

2.3.1. PEDOT based Na^+ and K^+ ion selective electrodes

The electrode fabrication procedures have been improved from those previously reported for the fabrication of PEDOT based Na^+ ion Selective Electrodes (ISEs) [16,17,19]. Furthermore, in this work, in addition to the Na^+ ISEs, analogous K^+ ISEs were also employed. Briefly, the electronically conductive layer (carbon ink) and dielectric layer were screen printed on Polyethylene terephthalate (PET) sheets. For the Poly(3,4-ethylenedioxythiophene) PEDOT formulations, PEDOT (~0.8 mg per electrode) was deposited on the exposed surfaces of the electrodes by constant-potential electro-polymerisation from 0.05 M solution of EDOT (97%) in EMIM NTf₂ (99.5%), using a three-electrode setup consisting of the carbon ink working electrode, a platinum wire counter electrode and a bare Ag wire as pseudo-reference electrode. Polymeric capping membranes were formed in the wells by drop-casting the THF-based cocktails. The cocktails for the Na^+ ion-selective electrode (Na^+ -ISE) and reference electrode (RE) used with the PEDOT interfacial layer were as previously reported [21]. The K^+ selective ISE cocktail was valinomycin (10% by weight), KTCBP (50% mol amount vs ionophore), and 1/2 ratio of PVC and plasticiser (DOS).

2.3.2. POT based Na^+ and K^+ ion selective electrodes

For the POT based Na^+ and K^+ ion selective electrodes both ISE and RE cocktails remained the same formulation as outlined with the addition of 10% by weight of POT directly to the membrane. These cocktails were used to prepare membranes with the same drop-casting protocol but removed the need for a separate mixed ion-electron conductivity layer with the PVC membrane deposited directly on the carbon ink sub-layer. Prior to drop-casting, a 20% solution of plasticiser (DOS for ISEs, 2 μL , DEHP for Res, 4 μL) in ethanol was added into the PMMA wells. The total amount of drop-cast membrane was 3.2 mg for the RE, and 1.4 mg for each of the ISEs (see Fig. 1).

2.4. Dropcasting automation

The deposition of the polymeric electrode membranes by drop casting is a labour-intensive process that can introduce sources of error which limit inter-electrode reproducibility. To try and address this issue, the drop casting procedure was automated via the use of an Opentrons® liquid handling robot (see Fig. 2). The robot was interfaced through an open source Python API, and a programme was developed in-house for automated drop casting of the electrode membranes. Different drop casting protocols were interactively defined through a graphical interface. After fabrication, each electrode was conditioned prior to use to facilitate hydration of the membranes and ensure equilibrium population of the membrane with the respective primary ions in the conditioning solution. This was achieved by immersing each electrode for 2 h in a 0.01 M solution of the primary ion (NaCl or KCl). Conditioning for shorter times or with lower concentrations resulted in a diminished response from the both the K^+ and Na^+ ISEs.

2.5. SwEatch platform

The 3D printed SwEatch pod-like platform previously reported [17] was redesigned to incorporate a dual macro-duct that provides for two-channel direct electrolyte monitoring in sweat. The main 3D printed platform assembly was a three-part design that enabled easy replacement of electronics, electrodes and sorbent material during use. The 3D printed platform was separated into three main components (Fig. 3); the microfluidic unit (Fig. 3A), platform body (Fig. 3B) and the fully integrated wearable platform (Fig. 3C). The microfluidic unit incorporated the dual macro duct and the two-half cylindrical arrangement of the sweat reservoir (Figs. 3 and 5A) which enabled two independent sample channels for the sodium and potassium electrodes (Fig. 3 and A). The electrodes were secured in location to prevent

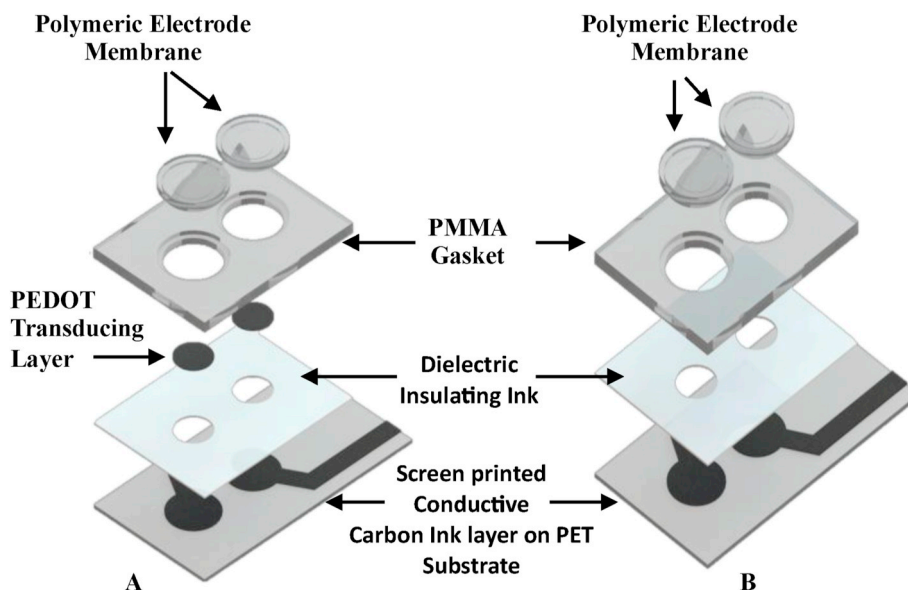


Fig. 1. Exploded view of the individual components of A. the combination PEDOT ISE electrode and B The combination POT ISE electrode.

longitudinal and lateral displacement during trials. This was achieved using flexible polymer TANGOBLACK contact pads to produce a snug fit between the lid and the macro-duct base (Fig. 3 1A). Redesign of the microfluidic 3D printed sub-assembly provided improved contact between the electrodes and the capillary flow of the sample in the fluidic channel. The multi-material 3D prints also enabled better sealing and close fit between the microfluidic unit and main platform body (Figs. 3 and 4B). The two-part body was held in place with a nylon M3XM12mm nut and bolt arrangement (Figs. 3 and 2B) in which the nut was counter-sunk flush with the surface. The platform employed a vertical arrangement of these units to enable the components to be arranged in a compact form factor. The platform held two Shimmer single channel PCBs, and two 3.7 V 155mAh batteries (Fig. 3 and B). The pebble shape added rigidity to the enclosed platform (Figs. 3 and 1C) by providing smooth design counters which avoid localised stress formation. The strap was fed through three loops located at the top and each side of the platform to ensure continuous contact with the skin and prevent movement during on-body trials.

2.6. On-body trials

The trials were conducted in association with the School of Health and Human Performance at DCU (full consent and ethical approval were obtained). The volunteer athlete was selected with a moderate to high fitness level. The fluidic device was primed by wetting the protruding thread with 30 μ L of deionised water and fastened onto the upper arm of the subject with elastic straps, after cleaning the skin

surface with a deionised/distilled water rinse and drying with a sterile gauze. On-body trials were carried out where the subject was exercising on a stationary bicycle for 90 min for the first and second trial, respectively. During each trial, contextual information such as the room temperature, humidity power exerted, arm movement and hydration regime were recorded. The amount of sweat collected was determined by weighing of the sorbent material before and after the trials. The electrodes were calibrated before and after the trials, and the potentiometric data was converted into analyte concentrations by applying the calibration data using a linear drift correction model.

3. Results and discussion

3.1. Electrode fabrication

During manual drop-casting a number of defects were observed in both the polymeric membranes (see S1 Fig. 1). The defects such as air bubbles and membrane overlapping resulted in high failure rates of the reference and ISEs (see Table 1). To combat this issue, the process was automated using the Opentrons[®] automated pipetting robot (see Fig. 3). This move toward automation resulted in a significantly reduced defect rate for both the reference and ISEs (Table 1).

The electrodeposition of a transducing layer of poly(3,4-ethylenedioxythiophene) (PEDOT) was also found to be a bottleneck in the fabrication as it requires up to 1 h per electrode and is not easily scalable. For this reason, we investigated the use of solution-processable alternative, specifically poly(4-octylthiophene) (POT) [20]. As

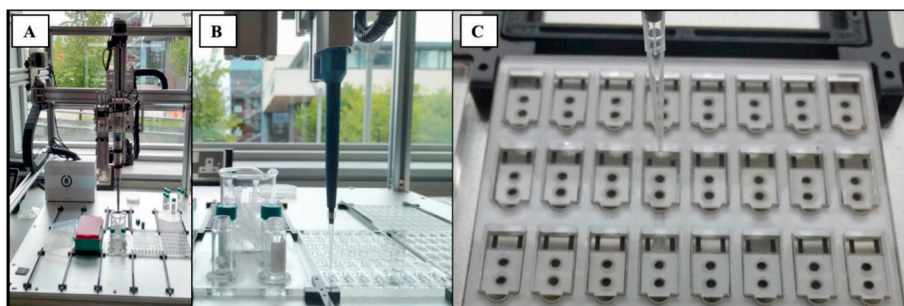


Fig. 2. Images showing A. the Opentrons[®] automated pipetting robot, B and C Showing the automated deposition of the polymeric electrode membranes (drop casting).

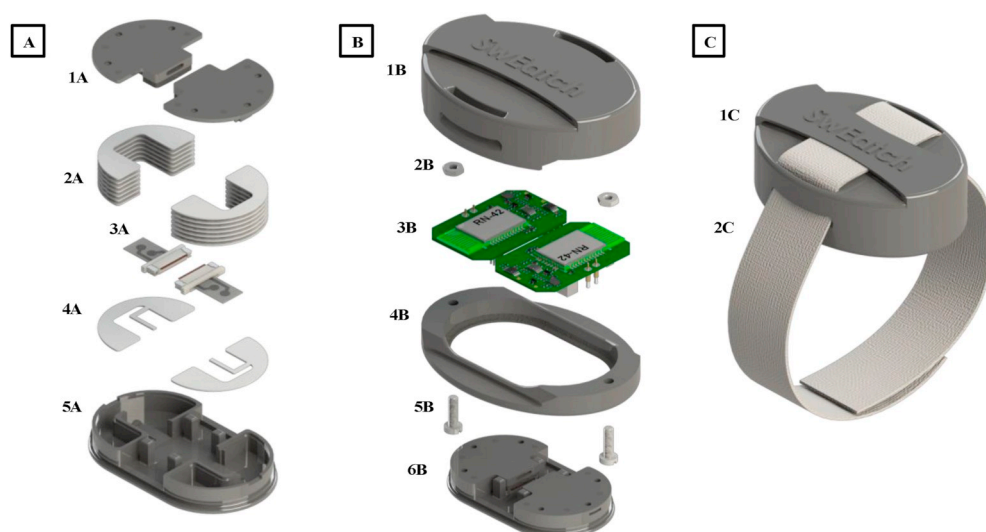


Fig. 3. A. Microfluidic unit; 1A. 3D printed lid using rigid polymer VEROBLACK with flexible polymer TANGOBLOCK contact pads, 2A. Sorbent material, 3A. K^+ and Na^+ ISEs, 4A. Sorbent material contact layer, 5A. sweat harvester. B. Platform body; 1B. 3D printed platform body, 2B and 5B. nylon M3XM12mm nut and bolt arrangement 3B. Shimmer single channel PCBs, 2×3.7 V 155mAh battery, 4B. sealing and press fit connector, 6B. Microfluidic unit, C. 1C Fully enclosed 3D printed Swatch platform, 2C. Platform strap.

Table 1

Rate of observed defects in the electrode membranes, fabricated by manual versus automated drop-casting.

Membrane type	Defect rate, manual drop-casting	Defect rate, automated drop-casting	p-value ^a
Reference	32/74 (43%)	8/82 (10%)	$1.40 \cdot 10^{-6}$
Na^+ ISE	19/50 (38%)	6/66 (9%)	$2.00 \cdot 10^{-4}$
K^+ ISE	29/62 (47%)	4/40 (10%)	$6.54 \cdot 10^{-5}$

^a p-values of one-sided Fisher's exact test.

mentioned above, for these electrodes, the mixed conduction polymer is added as a component of the membranes in a 10% content by mass, and the soft polymeric membrane formed directly on top of the carbon ink sub-layer, without creating a distinct interfacial transduction layer. This further simplified the fabrication process through integration of the mixed conduction and ion recognition layers into a single hybrid layer.

3.2. Characterisation of electrode response

Na^+ ISEs based on the calixarene ionophore, K^+ ISEs based on valinomycin, and REs based on the ionic liquid 1-Hexyl-3-methylimidazolium tris-(pentafluoroethyl)trifluorophosphate (HMIM FAP) [21], were first characterised using a commercial Ag/AgCl reference

electrode in solutions with log ionic activity ranging from -4.0 to -1.0. The REs demonstrated a stable potential over all concentration ranges which can be expected to be encountered in sweat. The Na^+ ISEs incorporating PEDOT exhibited a linear response to Na^+ over the range $\log(a) = -4.0$ to -1.0 , with slopes of 52.4 ± 6.3 mV/decade ($n = 8$). The sensitivity of the corresponding K^+ PEDOT electrodes was found to be somewhat lower at 45.7 ± 7.4 mV/decade ($n = 8$), with a linear range from $\log(a) = -4.0$ to -0.5 . The POT based formulations showed improved sensitivity in the $\log(a) = -4.0$ to -1.0 range, specifically 56.4 ± 2.2 mV/decade for the Na^+ ISE, and 54.3 ± 1.5 mV/decade for the K^+ ISE ($n = 8$ in both cases). In the following sections, we focus particularly on the characteristics of the POT based electrodes, to explore whether the hybrid layer configuration affects the electrode performance.

3.3. Stability and selectivity

Following initial characterisation described above, the selectivity and stability of the electrodes was examined in the presence of the most relevant interferents for the application, that is, Na^+ and K^+ , followed by H^+ , Mg^{2+} and Ca^{2+} [22,23]. A calibration experiment in which the response of the ISEs and of the RE to alternating additions of NaCl and KCl were recorded (Fig. 4, A). Each step corresponds to an increase in $\log(a_{M+})$ of either Na^+ or K^+ of 0.5 M, calculated using the Debye-

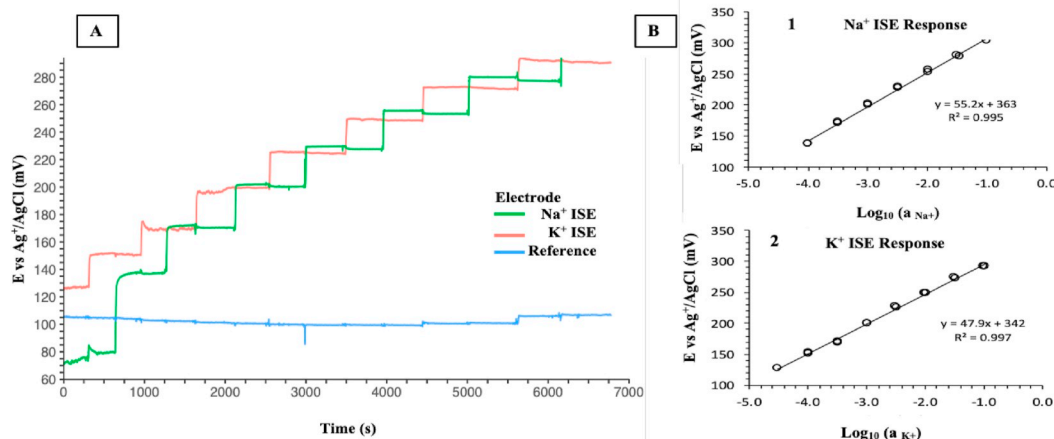


Fig. 4. A. Response of (POT) Na^+ ISE, K^+ ISE and RE to increasing concentrations of NaCl and KCl B. Linear responses of the Na^+ (1.) and K^+ (2.), ISEs in mixed electrolyte solutions, activities determined by Debye-Hückel model.

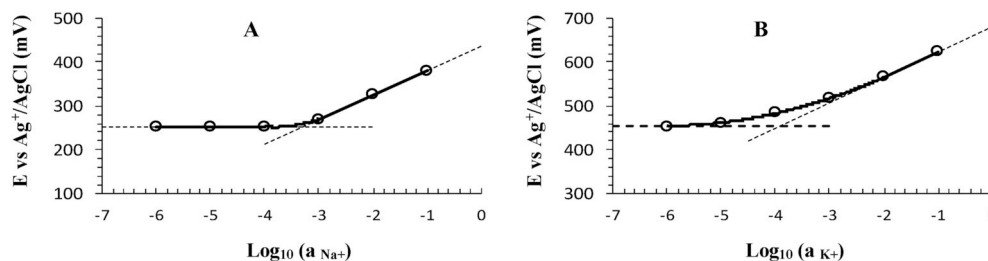


Fig. 5. Fixed interference method for the determination of selectivity coefficients. A: Response of an Na^+ ISE to successive additions of NaCl in a fixed background concentration of KCl of 0.1 mol/L; B: response of a K^+ ISE to successive additions of KCl in a fixed background concentration of NaCl of 0.1 mol/L.

Hückel model. Each ISE displayed a rapid response even in the mixed analyte solution, with no evidence of cross-response, and reasonable sensitivity (Fig. 4, B). The potentiometric selectivity coefficients (Fig. 5) were determined via the fixed interference method, with a background concentration of interferent of 0.1 mol/L [24], giving values of $\log K_{\text{Na}^+, \text{K}^+}^{\text{pot}} = -2.7 \pm 0.1$ or the Na^+ ISE ($n = 8$) and $\log K_{\text{K}^+, \text{Na}^+}^{\text{pot}} = -2.1 \pm 0.1$ for the K^+ ISE ($n = 8$).

The response to other interferents was probed by performing 4-point calibrations with salts (NaCl , KCl , MgCl_2 , $\text{Ca}(\text{NO}_3)_2$), and strong acid (HCl) (See Fig. 6). The potential of the electrodes is almost completely independent of the concentrations of these interferents, except at very high concentrations (0.1 M) which will not be encountered in the application. Human sweat typically has concentrations of Na^+ in the range $10^{-2} - 10^{-1}$ M, K^+ in the range $3 - 10 \cdot 10^{-3}$ M, and pH from 4.5 to 7 depending on the individual and method of sweat stimulation [22,23]. Other cations are found at much lower concentrations ($\text{Ca}^{2+} \approx 10^{-4}$ M, Mg^{2+} and $\text{Zn}^{2+} \approx 10^{-5}$ M). Three different simulated sweat compositions (sSweat) were investigated that mimic the composition of thermogenic human sweat: 1. sSweat A: $c_{\text{NaCl}} = 0.04$ mol/L, $c_{\text{KCl}} = 0.005$ mol/L; 2. sSweat B: $c_{\text{NaCl}} = 0.04$ mol/L, $c_{\text{KCl}} = 0.005$ mol/L, $c_{\text{Ca}(\text{NO}_3)_2} = 4 \cdot 10^{-7}$ mol/L, $c_{\text{MgCl}_2} = 4 \cdot 10^{-8}$ mol/L; 3. sSweat C: $c_{\text{NaCl}} = 0.04$ mol/L, $c_{\text{K}_2\text{HPO}_4} = 0.0024$ mol/L, $c_{\text{K}_2\text{HPO}_4} = 0.0476$ mol/L ($c_{\text{K}^+} = 0.00524$ mol/L, pH = 5.8). In the simulated Sweat C solution, a phosphate buffer was used to generate the slightly acidic pH which sometimes occurs in sweat.

The drift of a test batch of POT electrodes ($n = 71$) was measured consecutively for a period of 2 h in each solution. The results are reported in Table 2, for the Na^+ ISEs, K^+ ISEs, and REs. The Ag/AgCl reference was shown to be stable (< 1.0 mV/h) under the same conditions, by measuring its potential against a standard calomel reference electrode. Most electrodes presented a modest drift, with a random distribution varying randomly from one electrode to the next. Given the low magnitude of the drift over the typical period of an exercise event,

Table 2

Summary of median drift for the RE, Na^+ ISE and K^+ ISE membranes in each of the three simulated Sweat solutions ($n = 71$).

Electrode type	Simulated sweat	n	Drift (mV/h) ^a
RE	A	8	0.1 ± 1.5
RE	B	8	-1.5 ± 1.7
RE	C	8	0.4 ± 0.5
Na^+ ISE	A	8	-1.3 ± 2.1
Na^+ ISE	B	8	0.2 ± 1.7
Na^+ ISE	C	8	-1.1 ± 2.2
K^+ ISE	A	7 ^b	-4.7 ± 4.7
K^+ ISE	B	8	0.0 ± 0.2
K^+ ISE	C	8	-0.9 ± 1.6

^a Reported as median \pm median absolute deviation.

^b One extreme outlier due to electrode failure was excluded.

the electrodes were deemed to have satisfactory stability for on-body measurements. Prior to unbody measurements the sensors were stored dry in the dark and re-calibrated before use as previously reported [18].

3.4. Fluidic design

The uptake and transport of the sweat, within the dual macro-duct, occurred in the same way as previously reported [17]. The mirrored fluidic unit was capable of drawing sweat from the skin through passive capillary action and bringing it into contact with both the Na^+ and K^+ combination electrodes (see supplementary information Fig. 3a). The flow rate is roughly constant with 1 or 2 threads (linear flow rate a ca., 1.0 and 7.0 $\mu\text{g}/\text{min}$ respectively), whereas with a triple thread, saturation behaviour occurs, with gradually decreasing flow rate from an initial high value of 26 $\mu\text{g}/\text{min}$ due to exhaustion of the available sample storage reservoir, which can accommodate up to 1.8g of sweat (See SI Fig. 3b). The use of a double thread was therefore judged to be

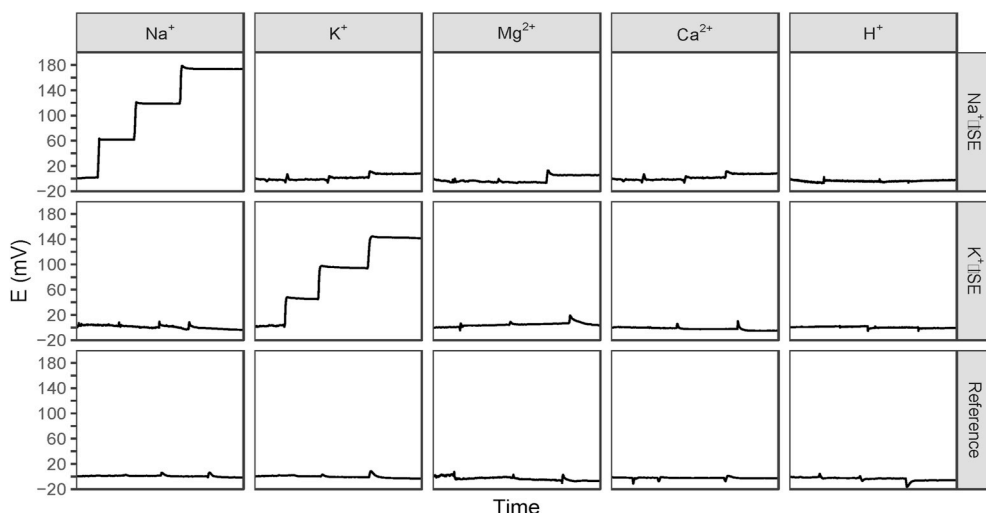


Fig. 6. Response of Na^+ ISE (top row), K^+ ISE (middle row) and RE (bottom row) to different analytes/interferents. The electrodes were exposed to increasing concentrations of analyte/interferent (10^{-4} , 10^{-3} , 10^{-2} , 10^{-1} mol/L). Addition times are indicated by the grey vertical lines. Initial potentials were normalised to $E = 0$.

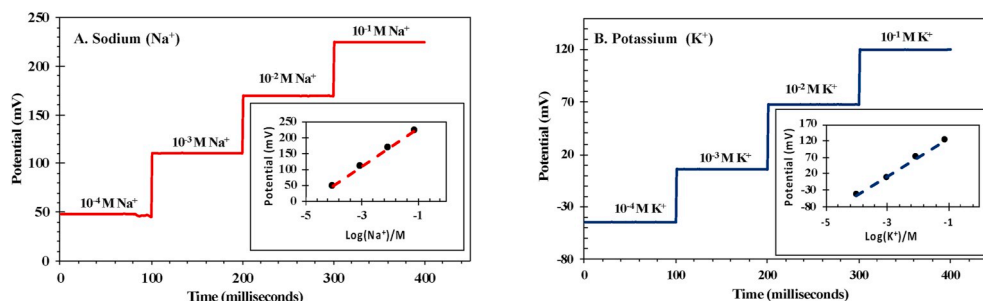


Fig. 7. Pre-Trial calibration of the SwEatch Platform for A Sodium Na^+ and B Potassium K^+ .

the most appropriate as it represents a medium to high sweat uptake which is greater than the expected rate of sweat generation reported for the sampling area and location [25,26]. The maximum rate of sample uptake into the SwEatch platform should be greater than the expected rate of sweat generation, in order to minimise sweat pooling at the skin contact area and ensure that there is minimal mixing from sweat emerging at varying times during on-body trials.

3.5. On-body trials

Four-point calibrations of the solid-state combination electrodes for Na^+ and K^+ (POT) electrodes were performed prior to commencing on-body trials. Calibrations for both Na^+ and K^+ were carried out by using 10^{-4} , 10^{-3} , 10^{-2} , 10^{-1} M NaCl and KCl. The known solutions were pipetted into the inlet of the platform where the thread brought the liquid in contact with the sorbent material at the reservoir which wicked the liquid across the Na^+ and K^+ combination electrodes. Results were transmitted to the laptop via Bluetooth and processed using the Consensys software by taking 100 data points from at each single decade interval (Fig. 7). The pre-trial slopes and intercepts for Na^+ were 61.13 mV/decade, 293.74 mV and for K^+ were 57.61 mV/decade, 183.78 mV, respectively.

During the trials, the SwEatch device was placed on the athlete's upper arm (Fig. 8) as this site produces significant sweat while also restricting movement of the device during the trial. The volunteer cycled for 90 min with an average speed of 33.8 km h^{-1} at an effort of 149–159 W leading to profuse sweating from the individual during the session. The volunteer's heart rate was also monitored throughout the trial (mean = 156 bpm), and the temperature in the room was kept relatively constant at 25.5°C and 19.1%, respectively (additional information can be found in [supplementary information Table 1](#)).

The outputs of the fully integrated SwEatch platform measuring Na^+ and K^+ for the duration of the session are shown in Fig. 9. The data clearly shows the sharp increase in the signal for both Na^+ and K^+ corresponding to sweat reaching both electrodes at ca. 8 min as previously reported [16,17,27]. For Na^+ after the initial rise the signal remains relatively stable from ca. 11 min with a slight increase at ca. 34 min until ca. 48 min at which time the signal starts to decline. This response pattern for Na^+ is consistent with what we and others have previously published [8,17,28] during on-body trials. However, the equivalent concentration range for Na^+ was slightly below the typical physiological range (10 mM–90 mM Na^+) [29]. The Na^+ concentration showed the expected increase from a baseline of 0.03 mM (1) to 1.89 mM (2) corresponding to sweat entering the device at ca. 8 min. The concentration rises to 2.97 mM at ca. 34 min (3) before decreasing to 2.21 mM (4) at ca. 58 min and further to 0.61 mM (5) at ca. 78 min. The low concentration observed in Na^+ levels throughout the trail can be attributed to a number of factors which include; the subjects sweating rate, skin temperature, electrolyte reabsorption amongst others. Further validation of the SwEatch platform against the 'gold standard analytical techniques' combined with increased trials are planned to fully assess the patterns observed. This will therefore allow



Fig. 8. Image showing the positioning SwEatch platform and visible sweating during the on-body trials.

us to further elucidate the potential of these type of wearable platforms to provide reliable data on the mechanisms of sweating and the physiology status.

For K^+ the results also showed increase in concentration from a baseline of 0.13 mM (1) to 3.31 mM (2) at ca. 11 min again corresponding to the introduction of sweat into the SwEatch platform, the slight differences in time reflecting the slightly different sweat transfer rates through the device pathways to each sensor. The concentration starts to decrease after ca. 14 min to a low of 1.65 mM (3) after which the concentration increases to 2.63 mM (4) at ca. 52 min and further to 7.25 mM (5) at ca. 88 min. This concentration range falls within the typical physiological range reported for K^+ (between 2 and 10 mM) [29]. No significant movement artefact was observed when the subject raised the arm to which the SwEatch platform was attached at ca. 18 min and at ca. 46 min, suggesting that the improved design is more robust to movement previously reported [16,17]. To confirm the stability of the electrode during the trials, post-trial calibrations were compared to pre-trial calibrations (Fig. 10). Virtually no change was

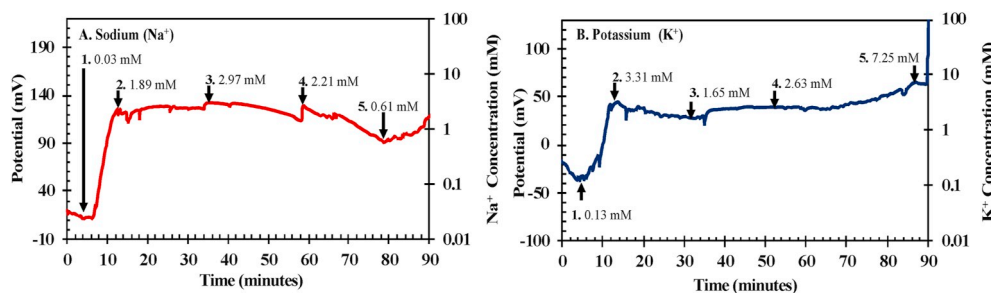


Fig. 9. The SwEatch platform outputs for the duration of the 90 min on-body trial.

exhibited, indicating that the electrode response remained stable throughout the trial. These results add to the body of knowledge of sweat electrolyte monitoring using on-body devices. Given that the electrodes appeared to be inherently stable over the course of the trials, and movement artefact was significantly reduced, there can be a certain degree of confidence in reliability of the signals obtained. An integrated calibration facility that can provide in-trial validation measurements at regular intervals would be ideal, but this is difficult to achieve practically, as it would involve storing at least one on-device standard, and switching this into contact with the electrodes, increasing the fluidic system/electronics complexity. Such added functionality may become available as fluidics based on biomimetic principles become more available and mature. Alternatively, it may be possible to periodically perturb the electrodes using an impressed signal e.g. apply a voltage and check current obtained in the presence of the sample to estimate the system impedance/resistance.

Over time, as more groups publish trial-based data using on-body chemical sensors, the patterns of electrolyte concentration variations in sweat during exercise will become much more established and contribute to a clearer interpretation of the physiological basis of these patterns. This will be part of a much bigger effort to expand real-time measurements using a wide range of on-body biochemical sensing, as is already happening with on-body patch-type sensing of glucose for personalised diabetes management [30].

4. Conclusion

In summary we have demonstrated the use of a wearable platform for the simultaneous detection of Na^+ and K^+ in sweat. The platform presented has differentiating factors compared to previously developed SwEatch platforms [17,31] such as simpler and partially automated electrode fabrication, improved electrode stability, platform redesign to accommodate two-channel direct electrolyte monitoring in sweat and resistance to movement artefact. This combination of changes to the platform have generated a new set of real-time data for measuring electrolytes in sweat in high performance athletes. However, it is acknowledged that these results should be interpreted with caution as the use of such technologies can be the source of unwanted variability in sweat monitoring. Increased validation of the response patterns obtained for electrolyte variations is required to establish if these

variations are real or accurate. Validation of the response patterns will only emerge when a substantial body of trial-based time series becomes available that exhibit similar trends. Establishing the true concentration ranges will require further creative thinking to address how to perform parallel measurements ideally on-device (same sample) during on-body trials.

Author contribution

Paolo Pirovano developed the automated fabrication process of the ISEs assisted in data processing and on-body trials, **Margaret McCaul** **Matthew Dorrian** contributed to the electrode fabrication and data processing, **Akshay Shinde** assisted in the design and fabricated the 3D printed SwEatch platform, **Margaret McCaul** co-ordinated the on-body trials, **Andrew Donohoe** assisted in the on-body trials and data processing, **Aidan J. Brady** and **Niall M Moyna** planned and conducted the on-body trials and assisted with writing the manuscript. **Gordon Wallace** and **Dermot Diamond** conceived the original idea. **Dermot Diamond** and **Margaret McCaul** contributed to the design and implementation of the research, to the analysis of the results. **Margaret McCaul** wrote the manuscript with inputs from all authors.

Declaration of competing interest

The authors declare that they have no known competing financial interests or personal relationships that could have appeared to influence the work reported in this paper.

Acknowledgements

This research was funded by Enterprise Ireland [grant number IP-2016-0504] and Science Foundation Ireland through the INSIGHT Centre grant number SFI/12/RC/2289_P2. Support from the Australian Research Council ACES Centre at the University of Wollongong is also acknowledged. 3D printing, laser cutting, and screen-printing was carried out at the Nano Research Facility in Dublin City University, which was funded under the Programme for Research in Third Level Institutions (PRTL) Cycle 5. The PRTL is co-funded through the European Regional Development Fund (ERDF), part of the European

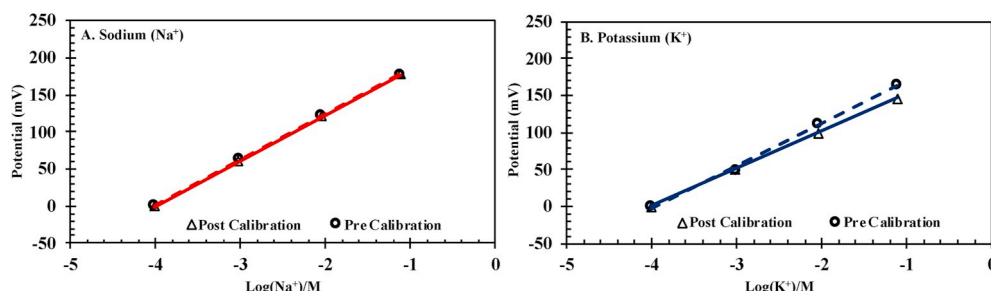


Fig. 10. A Pre and Post trial calibration of the Sodium Combination Electrodes and B Pre and post-trial calibrations for Potassium combination electrodes.

Union Structural Funds Programme 2011–2015. In addition, we acknowledge Norman Davidson and Paddy White of Shimmer Technologies for their assistance in this work.

Appendix A. Supplementary data

Supplementary data to this article can be found online at <https://doi.org/10.1016/j.talanta.2020.121145>

References

- [1] M.C. Brothers, M. DeBrosse, C.C. Grigsby, R.R. Naik, S.M. Hussain, J. Heikenfeld, S.S. Kim, Achievements and challenges for real-time sensing of analytes in sweat within wearable platforms, *Acc. Chem. Res.* 52 (2019) 297–306, <https://doi.org/10.1021/acs.accounts.8b00555>.
- [2] A.J. Bandonkar, W.J. Jeang, R. Ghaffari, J.A. Rogers, Wearable sensors for biochemical sweat analysis, *Annu. Rev. Anal. Chem.* 12 (2019) 1–22, <https://doi.org/10.1146/annurev-anchem-061318-114910>.
- [3] M. McCaul, T. Glennon, D. Diamond, Challenges and opportunities in wearable technology for biochemical analysis in sweat, *Current Opinion in Electrochemistry* 3 (2017) 46–50, <https://doi.org/10.1016/j.coelec.2017.06.001>.
- [4] J. Heikenfeld, A. Jajack, J. Rogers, P. Gutruf, L. Tian, T. Pan, R. Li, M. Khine, J. Kim, J. Wang, J. Kim, Wearable sensors: modalities, challenges, and prospects, *Lab Chip* 18 (2018) 217–248, <https://doi.org/10.1039/C7LC00914C>.
- [5] A.J. Bandonkar, J. Wang, Non-invasive wearable electrochemical sensors: a review, *Trends Biotechnol.* 32 (2014) 363–371, <https://doi.org/10.1016/j.tibtech.2014.04.005>.
- [6] E. Scurati-Manzoni, E.F. Fossali, C. Agostoni, E. Riva, G.D. Simonetti, M. Zanolari-Calderari, M.G. Bianchetti, S.A.G. Lava, Electrolyte abnormalities in cystic fibrosis: systematic review of the literature, *Pediatr. Nephrol.* 29 (2014) 1015–1023, <https://doi.org/10.1007/s00467-013-2712-4>.
- [7] S.N. Cheuvront, R. Carter, M.N. Sawka, Fluid balance and endurance exercise performance, *Curr. Sports Med. Rep.* 2 (2003) 202–208.
- [8] H.Y.Y. Nyein, M. Bariya, L. Kivimäki, S. Uusitalo, T.S. Liaw, E. Jansson, C.H. Ahn, J.A. Hangasky, J. Zhao, Y. Lin, T. Happonen, M. Chao, C. Liedert, Y. Zhao, L.-C. Tai, J. Hiltunen, A. Javey, Regional and correlative sweat analysis using high-throughput microfluidic sensing patches toward decoding sweat, *Science Advances* 5 (2019) eaaw9906, <https://doi.org/10.1126/sciadv.aaw9906>.
- [9] H.Y.Y. Nyein, L.-C. Tai, Q.P. Ngo, M. Chao, G.B. Zhang, W. Gao, M. Bariya, J. Bullock, H. Kim, H.M. Fahad, A. Javey, A wearable microfluidic sensing patch for dynamic sweat secretion analysis, *ACS Sens.* 3 (2018) 944–952, <https://doi.org/10.1021/acssensors.7b00961>.
- [10] M. Parrilla, I. Ortiz-Gómez, R. Cánovas, A. Salinas-Castillo, M. Cuartero, G.A. Crespo, Wearable potentiometric ion patch for on-body electrolyte monitoring in sweat: toward a validation strategy to ensure physiological relevance, *Anal. Chem.* 91 (2019) 8644–8651, <https://doi.org/10.1021/acs.analchem.9b02126>.
- [11] A. Zoerner, S. Oertel, M.P.M. Jank, L. Frey, B. Langenstein, T. Bertsch, Human sweat analysis using a portable device based on a screen-printed electrolyte sensor, *Electroanalysis* 30 (2018) 665–671, <https://doi.org/10.1002/elan.201700672>.
- [12] R. Hoekstra, P. Blondeau, F.J. Andrade, IonSens: a wearable potentiometric sensor patch for monitoring total ion content in sweat, *Electroanalysis* 30 (2018) 1536–1544, <https://doi.org/10.1002/elan.201800128>.
- [13] A. Hauke, P. Simmers, Y.R. Ojha, B.D. Cameron, R. Ballweg, T. Zhang, N. Twine, M. Brothers, E. Gomez, J. Heikenfeld, Complete validation of a continuous and blood-correlated sweat biosensing device with integrated sweat stimulation, *Lab Chip* 18 (2018) 3750–3759, <https://doi.org/10.1039/C8LC01082J>.
- [14] Y.-L. Liu, R. Liu, Y. Qin, Q.-F. Qiu, Z. Chen, S.-B. Cheng, W.-H. Huang, Flexible electrochemical urea sensor based on surface molecularly imprinted nanotubes for detection of human sweat, *Anal. Chem.* 90 (2018) 13081–13087, <https://doi.org/10.1021/acs.analchem.8b04223>.
- [15] L.-C. Tai, W. Gao, M. Chao, M. Bariya, Q.P. Ngo, Z. Shahpar, H.Y.Y. Nyein, H. Park, J. Sun, Y. Jung, E. Wu, H.M. Fahad, D.-H. Lien, H. Ota, G. Cho, A. Javey, Methylxanthine drug monitoring with wearable sweat sensors, *Adv. Mater.* 30 (2018) 1707442, <https://doi.org/10.1002/adma.201707442>.
- [16] T. Glennon, C. O'Quigley, M. McCaul, G. Matzeu, S. Beirne, G.G. Wallace, F. Stroeescu, N. O'Mahoney, P. White, D. Diamond, 'SWEATCH': a wearable platform for harvesting and analysing sweat sodium content, *Electroanalysis* 28 (2016) 1283–1289, <https://doi.org/10.1002/elan.201600106>.
- [17] M. McCaul, A. Porter, R. Barrett, P. White, F. Stroeescu, G. Wallace, D. Diamond, Wearable Platform for Real-Time Monitoring of Sodium in Sweat, *ChemPhysChem* (2018), <https://doi.org/10.1002/cphc.201701312>.
- [18] A. Alizadeh, A. Burns, R. Lenigk, R. Gettings, J. Ashe, A. Porter, M. McCaul, R. Barrett, D. Diamond, P. White, P. Skeath, M. Tomczak, A wearable patch for continuous monitoring of sweat electrolytes during exertion, *Lab Chip* 18 (2018) 2632–2641, <https://doi.org/10.1039/C8LC00510A>.
- [19] C. Zuliani, G. Matzeu, D. Diamond, A liquid-junction-free reference electrode based on a PEDOT solid-contact and ionogel capping membrane, *Talanta* 125 (2014) 58–64, <https://doi.org/10.1016/j.talanta.2014.02.018>.
- [20] A. Michalska, Optimizing the analytical performance and construction of ion-selective electrodes with conducting polymer-based ion-to-electron transducers, *Anal. Bioanal. Chem.* 384 (2006) 391–406, <https://doi.org/10.1007/s00216-005-0132-4>.
- [21] D. Diamond, G. SVEHLab, E.M. Seward, M.A. McKERVEY, A SODIUM ION-SELECTIVE ELECTRODE BASED ON METHYL p-BUTYL CALIX[4]ARYL ACETATE AS THE IONOPHORE, (n.d.) 9.
- [22] F. Herrmann, L. Mandol, Studies of pH of sweat produced by different forms of stimulation*, *J. Invest. Dermatol.* 24 (1955) 225–246, <https://doi.org/10.1038/jid.1955.36>.
- [23] S.J. Montain, S.N. Cheuvront, H.C. Lukaski, Sweat mineral-element responses during 7 h of exercise-heat stress, *Int. J. Sport Nutr. Exerc. Metabol.* 17 (2007) 574–582, <https://doi.org/10.1123/ijnsnem.17.6.574>.
- [24] C. Bieg, K. Fuchsberger, M. Stelzle, Introduction to polymer-based solid-contact ion-selective electrodes—basic concepts, practical considerations, and current research topics, *Anal. Bioanal. Chem.* 409 (2017) 45–61, <https://doi.org/10.1007/s00216-016-9945-6>.
- [25] C.J. Smith, G. Havenith, Body mapping of sweating patterns in male athletes in mild exercise-induced hyperthermia, *Eur. J. Appl. Physiol.* 111 (2011) 1391–1404, <https://doi.org/10.1007/s00421-010-1744-8>.
- [26] G. Havenith, A. Fogarty, R. Bartlett, C.J. Smith, V. Ventenat, Male and female upper body sweat distribution during running measured with technical absorbents, *Eur. J. Appl. Physiol.* 104 (2008) 245–255, <https://doi.org/10.1007/s00421-007-0636-z>.
- [27] A. Alizadeh, A. Burns, R. Lenigk, R. Gettings, J. Ashe, A. Porter, M. McCaul, R. Barrett, D. Diamond, P. White, P. Skeath, M. Tomczak, A wearable patch for continuous monitoring of sweat electrolytes during exertion, *Lab Chip* 18 (2018) 2632–2641, <https://doi.org/10.1039/C8LC00510A>.
- [28] W. Gao, S. Emaminejad, H.Y.Y. Nyein, S. Challa, K. Chen, A. Peck, H.M. Fahad, H. Ota, H. Shiraki, D. Kiriya, D.-H. Lien, G.A. Brooks, R.W. Davis, A. Javey, Fully integrated wearable sensor arrays for multiplexed in situ perspiration analysis, *Nature* 529 (2016) 509–514, <https://doi.org/10.1038/nature16521>.
- [29] L.B. Baker, Sweating rate and sweat sodium concentration in athletes: a review of methodology and intra/interindividual variability, *Sports Med.* 47 (2017) 111–128, <https://doi.org/10.1007/s40279-017-0691-5>.
- [30] FreeStyle Libre, Blood glucose monitoring system - diabetes care, n.d. <https://www.freestylelibre.co.uk/libre/index.html>, Accessed date: 26 April 2017.
- [31] T. Glennon, C. O'Quigley, M. McCaul, G. Matzeu, S. Beirne, G.G. Wallace, F. Stroeescu, N. O'Mahoney, P. White, D. Diamond, 'SWEATCH': a wearable platform for harvesting and analysing sweat sodium content, *Electroanalysis* 28 (2016) 1283–1289, <https://doi.org/10.1002/elan.201600106>.